

## Detection of a low frequency quasi-periodic oscillation in the soft state of Cygnus X-1 with Insight-HXMT

ZHEN YAN,<sup>1</sup> STEFANO RAPISARDA,<sup>1</sup> AND WENFEI YU<sup>1</sup>

<sup>1</sup>*Shanghai Astronomical Observatory, Chinese Academy of Sciences,  
80 Nandan Road, Shanghai 200030, China*

### ABSTRACT

We report the detection of a short-lived narrow quasi-periodic oscillation (QPO) at  $\sim 88$  mHz in an Insight-HXMT observation during the soft state of the persistent black hole high-mass X-ray binary Cygnus X-1. This QPO is significantly detected in all the three instruments of Insight-HXMT, so in the broad energy range 1-250 keV. The fractional rms of the QPO does not show significant variations above 3 keV ( $\sim 5\%$ ) while it decreases at lower energy ( $\sim 2\%$ ). We show that this QPO is different from the type-A, -B, and -C QPOs usually observed in black hole X-ray binaries. We compare QPOs at similar frequencies that have been previously detected in other persistent high mass X-ray binaries in the soft state; we speculate that such QPOs might relate to some local inhomogeneity rarely formed in the accretion flow of wind-fed accretion systems.

*Keywords:* accretion, accretion disks - stars: black holes - X-rays: binaries

### 1. INTRODUCTION

Cygnus X-1 is a bright persistent X-ray binary consisting of a black hole accreting matter from an OB star (Bowyer et al. 1965; Bolton 1972; Webster & Murdin 1972). Since its discovery, Cygnus X-1 has been the target of extensive multiwavelength observational campaigns (e.g. Herrero et al. 1995; Nowak et al. 1999; Gallo et al. 2005; Albert et al. 2007; Grinberg et al. 2013; Kantzas et al. 2021), making it one of the most-studied X-ray sources. From the very early observations of Cygnus X-1, it was clear that the X-ray emission undergoes dramatic changes in spectral distribution and brightness (Tananbaum et al. 1972).

Analogous changes have been observed in most later discovered black hole X-ray binaries (BH XRBs) and have been classified into different accretion states (e.g. Remillard & McClintock 2006; Belloni 2010). The accretion states that have been first identified are the low-hard state (LHS) and the high-soft state (HSS). In the LHS, the energy spectrum can be described by a power law (the photon index  $\sim 1.5$ -2.1) and in the HSS by a multitemperature blackbody component. It is generally accepted that the multitemperature blackbody

emission arises from an accretion disk around the black hole (Shakura & Sunyaev 1973) and the power law is the result of Compton upscattering of cool photons by hot electrons close to the black hole (see reviews in Done et al. 2007; Yuan & Narayan 2014). Accretion states are also identified according to the timing properties of the source (see reviews by Remillard & McClintock 2006; Belloni 2010; Belloni & Stella 2014). The power density spectrum (PDS) in the LHS usually exhibits low-frequency quasi-periodic oscillations (LF QPOs,  $\sim 0.01$ -10 Hz) on top of broadband noise. QPOs are classified as type A, B, and C according to their frequency, amplitude, and coherence (see Wijnands et al. 1999; Casella et al. 2004, for detailed definitions of QPO types). Strong high-coherence type-C QPOs are usually observed in the LHS, when the total fractional rms amplitude is high ( $\sim 30\%$ ). In the HSS the amplitude of the variability drops dramatically ( $\lesssim 1\%$ ) and no QPOs are observed. The above phenomenon has been observed in almost every transient BH XRB, which has the largest population of known Galactic BHs. The LHS is usually observed at the beginning and the end of periods of enhanced accretion (outbursts), when the luminosity is low, while the HSS occurs at maximum luminosity. Between these two extremes, several transition states are also observed (Remillard & McClintock 2006; Belloni 2010).

However, some persistent BH XRBs can exhibit accretion states different from the transient BH XRBs. Cygnus X-1 is one of these sources, as its HSS is characterized by both multitemperature blackbody and Compton power law emission (e.g. Gierliński et al. 1999). The X-ray timing properties of accretion states in Cygnus X-1 differ from the general description mentioned above. Type-C QPOs have never been detected during the LHS of Cygnus X-1 (Grinberg et al. 2014; Ingram & Motta 2019) and the HSS shows high variability (fractional rms amplitude  $\sim 25\%$ ; Axelsson et al. 2005; Grinberg et al. 2014). However, there were broad and weak narrow QPOs detected in its PDS during different spectral states, which were sometimes called QPOs (e.g., Cui et al. 1997b; Paul et al. 1998; Pottschmidt et al. 2003; Axelsson et al. 2005; Shaposhnikov & Titarchuk 2006; Grinberg et al. 2014).

In this paper, we report the detection of a millihertz QPO in one of the Insight-HXMT observations of Cygnus X-1 during the soft state. In Section 2, we describe the data reduction, in Section 3 the spectral and timing analysis, and in Section 4 we compare the detected signal to similar signals observed in other BH XRBs and discuss possible physical scenarios.

## 2. OBSERVATIONS AND DATA REDUCTION

The Insight-Hard X-ray Modulation Telescope (HXMT) (Zhang et al. 2020) is the China’s first X-ray astronomy satellite. Insight-HXMT has three major scientific payloads: the Low Energy Telescope (LE, 1–10 keV), the Medium Energy Telescope (ME, 5–35 keV), and the High Energy Telescope (HE, 20–250 keV), capable of observations down to a time resolution of 1 ms,  $276\mu\text{s}$ , and  $25\mu\text{s}$ , respectively. The effective area of the three payloads is  $384\text{ cm}^2$ ,  $952\text{ cm}^2$ , and  $5000\text{ cm}^2$ , respectively.

In order to reduce the data file size, a long Insight-HXMT observation is man made, split into multiple segments. Each segment lasts approximately three hours, which is named as “exposure” and identified with an Exposure ID<sup>1</sup>. We analyzed the longest observation of Cygnus X-1 (Obs. ID P0101315001, start time 2017 August 24T02:49:21 UTC) in the Insight-HXMT data archive. The selected observation contains 13 exposures, for a total observation time of about 150 ks (see Figure 1).

We performed data reduction by using the Insight-HXMT Data Analysis Software package (HXMTDAS) V2.02. For all the three payloads, we extracted cleaned

events applying the following filtering criteria: (1) exclusion of time periods when Insight-HXMT passes through the South Atlantic Anomaly (T\_SAA > 300 && TN\_SAA > 300 && SAA\_FLAG == 0); (2) elevation angle >  $10^\circ$  (ELV > 10); (3) pointing offset angle <  $0.1^\circ$  (ANG\_DIST < 0.1); (4) cutoff rigidity > 8 GeV (COR > 8). An additional filtering criterion was applied for LE data: elevation angle from Earth bright limb >  $20^\circ$  (DYE\_ELV >  $20^\circ$ ). For LE, ME, and HE, we computed binned light curves, energy spectra, and corresponding background from cleaned event files using the HXMTDAS tools <le/me/he>lcgen, <le/me/he>specgen, and <le/me/he>bkgmap, respectively. In particular, we extracted source and background light curves with time resolution  $1/256$  ( $\approx 0.0039$ ) s in the energy band 1–10 keV, 5–30 keV, and 20–250 keV for LE, ME, and HE, respectively.

We also downloaded the daily light curves from the X-ray all-sky monitoring instruments Swift/BAT (Krimm et al. 2013) and MAXI (Matsuoka et al. 2009), selecting Swift/BAT and MAXI data simultaneous to our Insight-HXMT observation (MJD 57989; see Figure 2).

## 3. DATA ANALYSIS AND RESULTS

### 3.1. Timing Analysis

For each payload and exposure, we subtracted the background from the light curve, we divided the light curves into segments of 128 s, and, for each segment, we computed Leahy-normalized PDSs (Leahy et al. 1983) using the HEASARC tool powerspec (XRONOS package). PDSs were averaged, obtaining in this way a single PDS for each exposure. Because of the chosen time resolution and segment length, PDSs have frequency resolution  $d\nu = 1/128 = 0.0078125$  Hz and Nyquist frequency  $\nu_N = 128\text{Hz}$ .

Figure 1 shows the light curve with a time resolution of 100 s for each payload for the entire selected observation. We visually inspected PDSs for each exposure and find obvious QPO features in all three payloads during the first exposure (Exp. ID P010131500101-20170824-01-01; red region in Figure 1). In this exposure, the PDS of each payload is characterized by a power law broadband noise with a narrow feature on top of it at low frequency (Figure 3). This narrow feature appears to be more prominent at higher energies (ME and HE), and it is not present in any other exposures of the selected observation. To ascertain the presence of the narrow feature in the LE low-energy regime (1–10 keV), we performed the same data reduction and analysis described above in two sub-low-energy bands, 1–3 keV and 3–10 keV, respectively.

<sup>1</sup> <http://hxmtweb.ihep.ac.cn/SoftDoc/67.jhtml>

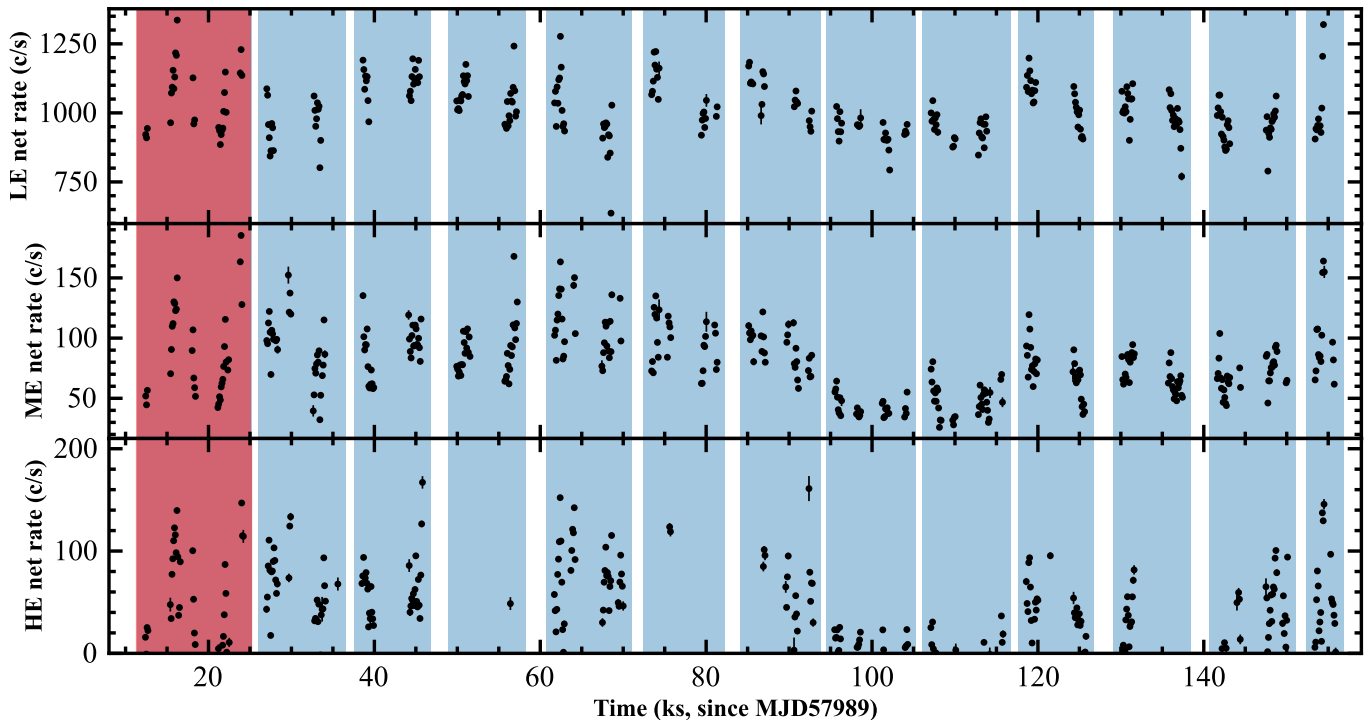


**Figure 1.** The light curves with a time resolution of 100 s during the Insight-HXMT observations for the three independent payloads: LE, ME and HE. Each exposure is marked by the shaded region. The red one is the exposure during which the QPO is detected.

We then subtracted the contribution from the Poisson noise, which was estimated by averaging Leahy-normalized PDSs above 100 Hz. The noise levels (1.99, 2.00, 1.99, 2.09 for LE 1–3 keV, LE 3–10 keV, ME, and HE) are consistent with the expected Poisson noise level in Leahy-normalized PDSs (Leahy et al. 1983). The average net count rate 870.50, 178.00, 87.04, and 52.60 counts/s for LE(1–3 keV), LE(3–10 keV), ME, and HE are used for calculating rms-normalized PDSs (Belloni & Hasinger 1990). The total fractional rms amplitude of each PSD is 11.4%, 27.3%, 28.7%, and 37.1% (below 32 Hz). We then fit the PDSs using a model consisting of a power law plus a narrow Lorentzian. The fitting was performed in XSPEC (Arnaud 1996). We obtained a statistically acceptable fit for the HE PDS (see Figure 3 and Table 1), while we noticed broad frequency residuals around 0.5 Hz for the LE and ME PDS. Adding a band-limited noise (BLN; a Lorentzian function with  $\nu_0$  fixed at 0) in the model, we obtain a statistically acceptable fit also for LE and ME (see Figure 3 and Table 1). We then calculate the  $\nu_{\max}$  ( $= \sqrt{\nu_0^2 + (FWHM/2)^2}$ ) to represent its characteristic frequency (e.g. Belloni et al. 2002), the values of which are  $0.50^{+0.07}_{-0.07}$ ,  $0.56^{+0.08}_{-0.07}$  and  $0.56^{+0.13}_{-0.11}$  for LE(1–3 keV), LE(3–10 keV), and ME data.

All the best-fitting parameters are listed in Table 1. The power-law noise with an index of  $\sim 1$  and the fractional rms are consistent with the soft state of Cygnus

X-1 (e.g. Cui et al. 1997a; Axelsson et al. 2005, 2006; Grinberg et al. 2014). A narrow QPO is detected in the all PDSs with significance of  $4.7\sigma$ ,  $6.8\sigma$ ,  $5.6\sigma$ , and  $6.3\sigma$  for the LE(1–3 keV), LE(3–10 keV), ME, and HE, respectively. The QPO frequencies at different energy bands are consistent within uncertainties; the averaged value is  $\sim 88$  mHz. The QPO is very narrow, especially at higher-energy bands (see the FWHM values in Table 1). The quality factors ( $Q = \nu_0/FWHM$ ) are  $10.8 \pm 7.7$ ,  $15.3 \pm 8.1$ ,  $> 13.7$ , and  $> 13$  for the LE(1–3 keV), LE(3–10 keV), ME, and HE, respectively. We further investigated the energy dependence of the QPO rms with more subenergy bands. We first produced the PDSs in the energy bands of 1–3 keV, 3–5 keV, 5–10 keV for LE data; 5–10 keV, 10–15 keV, 15–30 keV for ME data; and 30–50 keV, 50–150 keV for HE data. We then calculated the fractional rms of the QPO by fitting each PDS. The QPO rms becomes almost constant ( $\sim 5\%$ ) above 3 keV and up to at least 50 keV (see Figure 4).

### 3.2. Further assessing the significance of the QPO

The classical method to determine the detection level of a signal is based on the statistical properties of the white noise (van der Klis 1989). For an averaged PDS, the white-noise power follows a  $\chi^2$  distribution with  $2MW$  dof, where  $M$  is the number of averaged powers at a specific frequency and  $W$  is the number of averaged

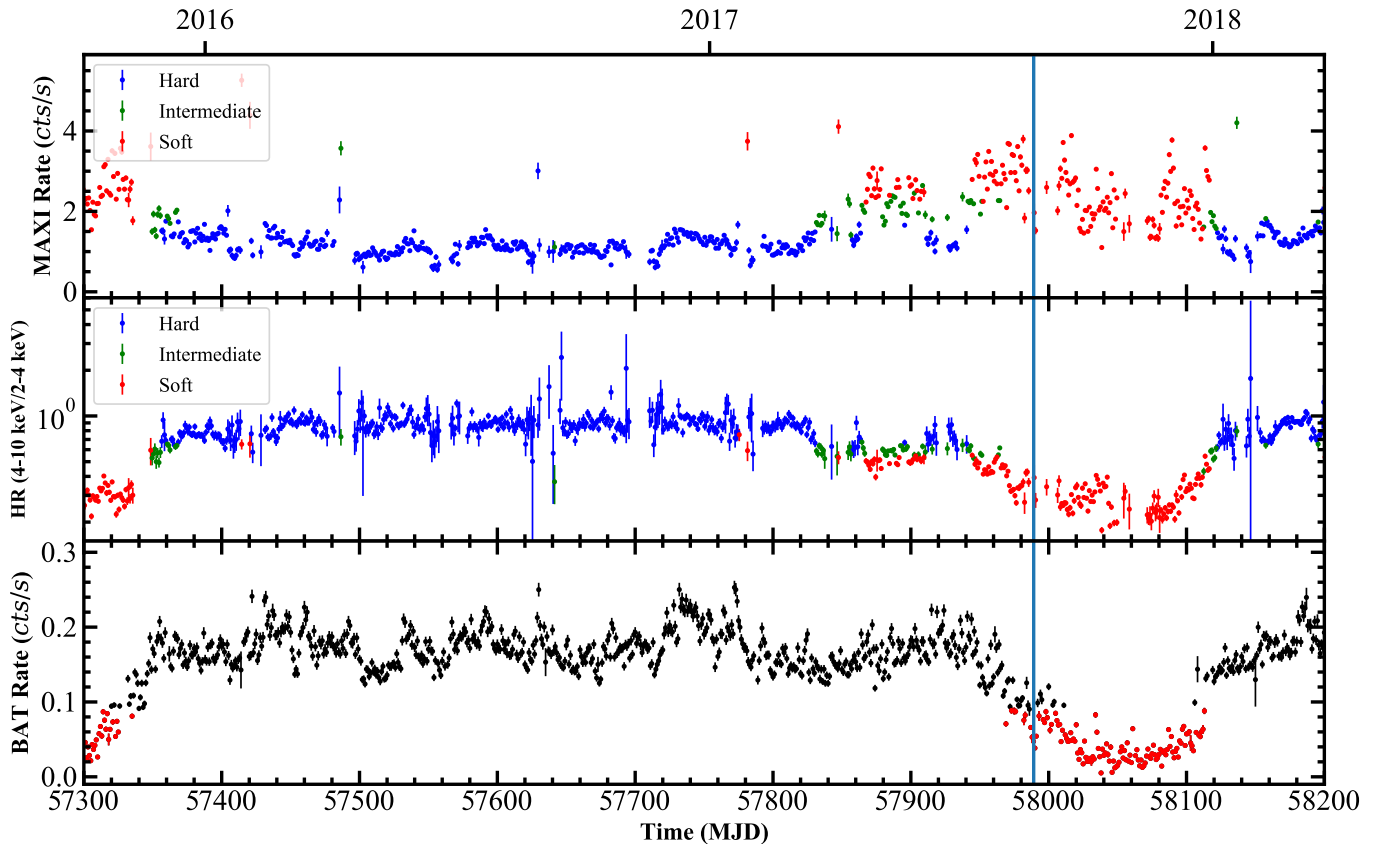


**Figure 2.** The daily light curves of Cygnus X-1 obtained from MAXI and Swift/BAT monitoring products. The definitions of X-ray spectral states are adopted from Grinberg et al. (2013). The vertical solid line marks the time of the Insight-HXMT observation we reported here.

**Table 1.** Best-fitting Parameters of the LE and ME PDSs

Component	Parameter	LE	LE	ME	HE
		(1–3keV)	(3–10keV)		
POW	Index	$1.16^{+0.04}_{-0.04}$	$1.08^{+0.03}_{-0.03}$	$1.08^{+0.04}_{-0.04}$	$0.95^{+0.02}_{-0.02}$
LOR	$\nu_0$ (mHz)	$89.27^{+5.68}_{-2.87}$	$86.91^{+1.47}_{-1.71}$	$87.53^{+1.70}_{-2.63}$	$88.84^{+0.72}_{-1.48}$
(QPO)	FWHM (mHz)	$14.03^{+15.53}_{-9.35}$	$7.39^{+4.86}_{-3.75}$	$2.88^{+3.62}_{-2.88}$	$2.64^{+4.19}_{-2.64}$
	rms(%)	$2.18^{+0.44}_{-0.47}$	$5.82^{+0.76}_{-0.87}$	$4.75^{+0.79}_{-0.91}$	$5.94^{+0.89}_{-0.94}$
LOR	$\nu_0$ (Hz)	0	0	0	...
(BLN)	FWHM (Hz)	$0.99^{+0.15}_{-0.13}$	$1.12^{+0.15}_{-0.13}$	$1.11^{+0.26}_{-0.22}$	...
	rms(%)	$5.57^{+0.39}_{-0.41}$	$14.31^{+0.74}_{-0.77}$	$13.39^{+1.12}_{-1.18}$	...
	$\chi^2/\text{dof}$	161.08/156	189.59/156	163.90/156	178.93/158

Note: The model is Powerlaw+Lorentzian+Lorentzian for LE and ME, Powerlaw+Lorentzian for HE. The uncertainties are the  $1\sigma$  ranges.

frequency bins. Integrating the  $\chi^2$  probability density function, it is possible to determine the  $p$ -value of a given power and define detection levels above the underlying noise. However, this method is not reliable for accessing detection above noise processes differing from white noise (Israel & Stella 1996; Vaughan 2005, 2010).

In our case, the QPO is detected in a frequency range dominated by red noise. To access the significance of the QPO with respect to the red noise, we applied the method proposed by Vaughan (2010) and implemented in the Python package *stingray* (Huppenkothen et al. 2019). We only considered the PDS below 8 Hz, where the red noise dominates. We fit-

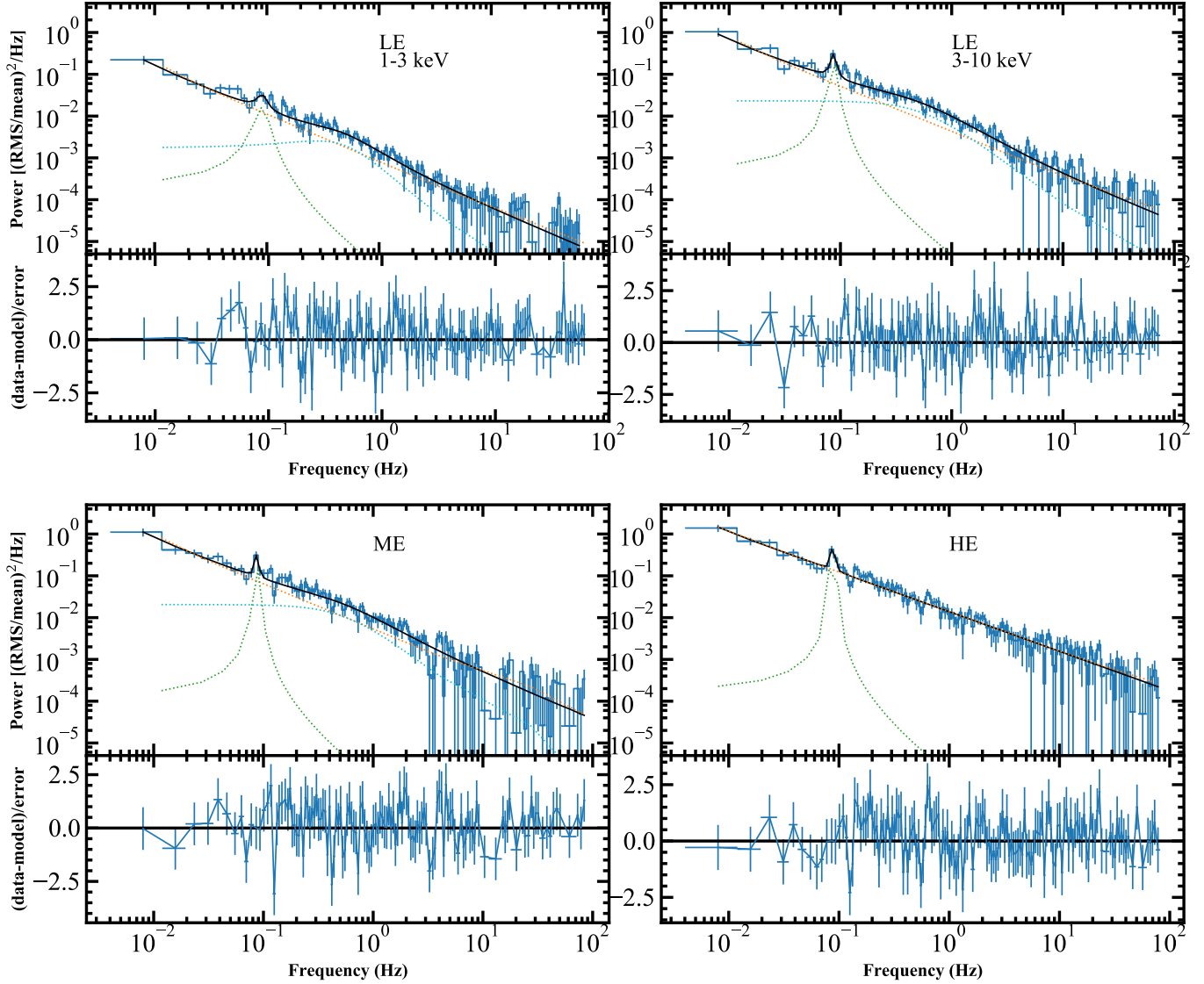


**Figure 3.** The PDSs of Cygnus X-1 of the LE, ME and HE on board the Insight-HXMT satellite. The solid black line is the best-fitting model of the PDS of each payload. The orange and green dotted lines show the power law component and the QPO. The cyan dotted line in the LE and ME subfigures is the BLN component. The lower panel of each subfigure is the ratio between residual and the error of the data.

ted the PDSs with a power-law function plus a constant and sample the model parameters with a Markov Chain Monte Carlo (MCMC) method in the `emcee` package (Foreman-Mackey et al. 2013). We then generated  $10^5$  fake PDSs using the sampled parameters, in order to derive a posterior probability distribution for the test statistics and thus a posterior predictive  $p$ -value. Our observed PDSs are averaged by  $M$  128s segments, where  $M$  is 18, 22, and 27 for LE, ME, and HE. We considered the  $M$  when generating the fake PDSs and did not rebin the fake PDSs. So, the derived  $p$ -value has been corrected for the number of periodograms searched including the number of segments and the number of frequencies.

We fitted each simulated PDS with a power-law plus a constant model and calculate  $(2I_j/S_j)$ , where  $I_j$  is the power at a given frequency  $f_j$  of a PDS and the  $S_j$  is the power from the model. We then plot the 99.450%, 99.730%, and 99.993% ( $2\sigma$ ,  $3\sigma$  and  $4\sigma$ ) significance levels, which is obtained from the  $10^5$  samples of the  $(2I_j/S_j)$  at each frequency (Figure 5). There is only one observed power at the frequency  $\sim 86$  mHz is larger than that of the 99.993% simulated PDS, which indicates a significant signal ( $> 4\sigma$ ) around this frequency in the PDS of LE(3–10keV), ME and HE. In the PDS of LE(1–3keV), the power at  $\sim 86$  mHz is marginally at  $2\sigma$ .

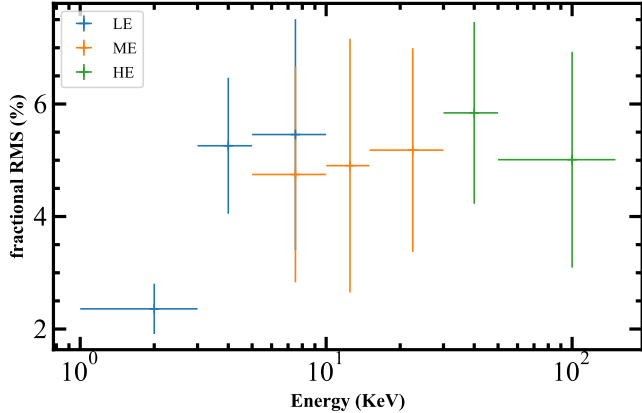


**Figure 4.** The fractional rms of the QPO as a function of photon energy. It becomes almost constant ( $\sim 5\%$ ) above 3 keV and extends to photon energies beyond 50 keV.

We first defined the test statistic  $T_R = \max(2I_j/S_j)$ . Then the  $p$ -values of the observed  $T_R^{obs}$  from the posterior probability distribution of  $T_R$  are 0.00394, 0.00334, and 0.00027 for LE (3–10 keV), ME, and HE, respectively Figure 6. The combined  $p$ -value of the three is  $7.45 \times 10^{-7}$  by using the Fisher method since they are independent tests for the three instruments. The frequency with maximum  $T_R$  from the three instruments are the same, so the  $p$ -value at this specific frequency should be smaller than the combined  $p$ -value (e.g. Huppenkothen et al. 2017), demonstrating a very significant signal of  $\sim 86$  mHz existing above the red noise.

We also used likelihood ratio test (LRT) to compare the two models with/and without a Lorentzian component. The likelihood ratio is defined as  $T_{LRT} = -2 \log(L_0/L_1)$ , where the  $L_0$  is the likelihood of the simple model and the  $L_1$  is the likelihood of the complex model. We fitted each simulated PDS with the two models and computed the  $T_{LRT}$ . The posterior probability distributions of the  $T_{LRT}$  can give us the  $p$ -values of  $T_{LRT}^{obs}$  are 0.00008, 0.00016, and 0.00001 for LE (3–10 keV), ME, and HE respectively Figure 6. Therefore, the statistics of  $T_R$  and  $T_{LRT}$  both demonstrate that a significant QPO detection in LE(3–10 keV), ME, and HE. The  $p$ -values of  $T_R$  and  $T_{LRT}$  of LE (1–3 keV) are at least one order of magnitude larger than those of higher-energy bands, which means the QPO is less significant below 3 keV.

### 3.3. Spectral and color analysis

We performed spectral analysis of the selected observation by combining the data from LE, ME, and HE. The effective areas of the three instruments have been calibrated using Crab nebula observations as described in Li et al. (2020). We jointly fit energy spectra of LE (1–10 keV), ME (8–30 keV), and HE (30–150 keV) with

the model `const*tbabs*(diskbb+reflkerr)` (see Figure 7), where abundances and cross sections of the absorption by the Galactic interstellar medium are set according to Wilms et al. (2000) and Verner et al. (1996). `reflkerr` is a relativistic reflection model that computes direct and reflection spectra assuming either a slab or a spherical plasma geometry (Niedźwiecki et al. 2019). In this framework, the Comptonization spectrum is computed with `compps` (Poutanen & Svensson 1996). We fix the black hole spin (0.99, Zhao et al. 2020, 2021), the inclination angle ( $27^\circ.5$ , Miller-Jones et al. 2021), and the index of the outer disk  $q_{out}$  (3), and we leave the inner disk index  $q_{in}$  and break radius  $R_{br}$  free (Fabian et al. 2012; Walton et al. 2016). We also tied the temperature of seed photons for Comptonization with the disk temperature. All of the best-fitting parameters are listed in Table 2. According to the electron temperature  $kT_e$  and optical depth  $\tau$  of the corona, we can derive the photon index of the Comptonization component (Zdziarski et al. 1996). The derived photon index  $\Gamma = 2.74 \pm 0.11$  and the best-fitting disk temperature  $T_{in} = 0.49 \pm 0.01$  keV are consistent with the soft state of Cygnus X-1 (Tomsick et al. 2014; Walton et al. 2016; Kawano et al. 2017; Lubiński et al. 2020). The unabsorbed X-ray flux (0.1–100 keV) is  $8.16 \times 10^{-8}$  ergs  $s^{-1}$   $cm^{-2}$ , which corresponds to  $\sim 2\%$  Eddington luminosity at a distance of 2.22 kpc and a BH mass  $21.2 M_\odot$  (Miller-Jones et al. 2021).

To confirm that Cygnus X-1 is in the soft state in our selected exposure, we computed count rates from swift/BAT and MAXI light curves simultaneous to our data (MJD 57989; see Figure 2). The count rate in the 15–50 keV (BAT) and 2–4 keV (MAXI) energy band is  $4.73 \pm 0.28 \times 10^{-2}$  counts  $cm^{-2}$   $s^{-1}$  and  $1.97 \pm 0.23$  counts  $s^{-1}$ , respectively. The corresponding hardness ratio (4–10 keV/2–4 keV) is  $0.39 \pm 0.08$ . According to the state classification criteria of Cygnus X-1 described in Grinberg et al. (2013), the observed X-ray intensity and hardness ratio are both consistent with the source being in the soft state.

## 4. DISCUSSION

We detected a very low-frequency ( $\sim 88$  mHz) QPO only during the first 12 ks of the longest Insight-HXMT observation of Cygnus X-1. This QPO is significantly detected in LE, ME, and HE, independently. The fractional rms amplitude is energy independent (above 3 keV; see Figure 4). The broadband noise at low frequency of the PDSs from all the three Insight-HXMT instruments is dominated by a power-law component with index  $\sim 1$  (Table 1), which is consistent with the soft state of Cygnus X-1 (e.g. Axelsson et al. 2005). The

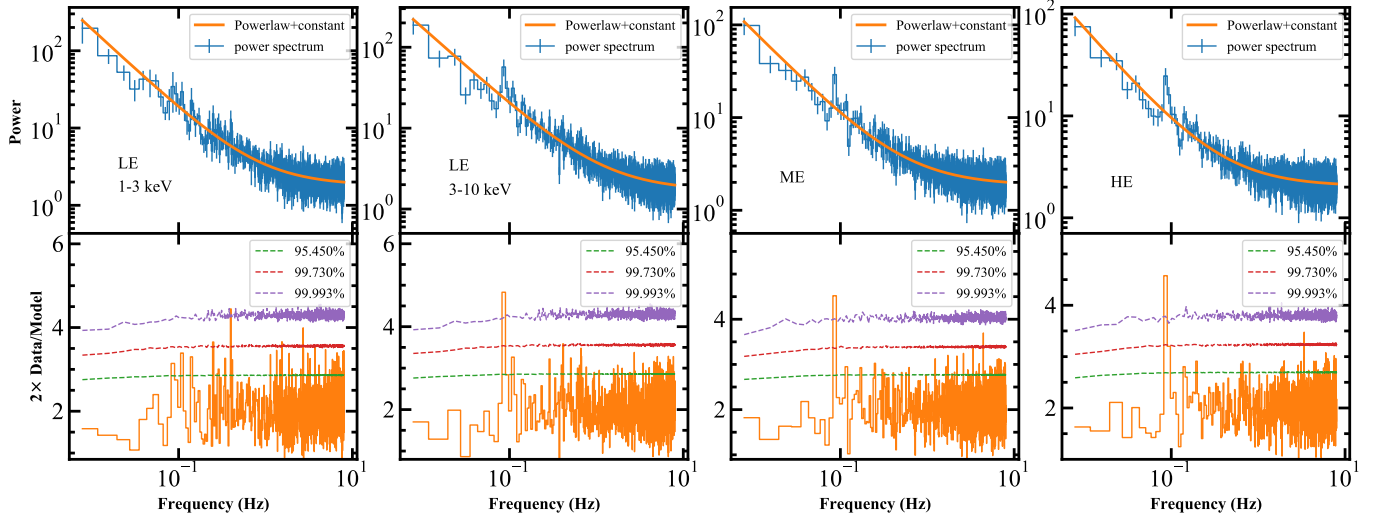


**Figure 5.** Upper panel: The PDS of LE (1–3keV), LE (3–10 keV), ME and HE. The orange line marks the best fitting model composed of a power law plus a constant. Lower panel: the ratio of the PDS data to the best-fitting power law model (the orange line in the upper panel). The green, red and purple dashed lines mark the levels at 95.450%, 99.730% and 99.993% of the simulated PDSs.

**Table 2.** Best-fitting parameters of the energy spectrum

Component	Parameter	Value
TBABS	$n_{\text{H}}$ [ $10^{22} \text{ cm}^{-1}$ ]	$0.46^{+0.04}_{-0.04}$
DISKBB	$kT_{\text{in}}$ [keV]	$0.49^{+0.01}_{-0.01}$
	Norm [ $10^4$ ]	$2.64^{+0.17}_{-0.19}$
REFLKERR	$q_{\text{in}}$	$7.52^{+0.58}_{-1.75}$
	$R_{\text{br}}$ [ $r_g$ ]	$3.29^{+0.23}_{-0.21}$
	$R_{\text{in}}$ [ $r_g$ ]	$2.22^{+0.10}_{-0.16}$
	$\tau$	$0.59^{+0.04}_{-0.03}$
	$A_{\text{fe}}$ [solar]	$< 10$
	$kT_e$ [keV]	$87.74^{+2.82}_{-2.39}$
	$\log \xi$ $\log[\text{erg cm s}^{-1}]$	$4.33^{+0.06}_{-0.03}$
	$f_{\text{refl}}$	$0.44^{+0.08}_{-0.07}$
$\chi^2/\text{dof}$		1332.78/1445

Note: The uncertainties are the  $1\sigma$  ranges.

measured fractional rms amplitude above 10 keV is more than two times larger than that below 3 keV (see subsection 3.1), which is also a characteristic of the soft state of Cygnus X-1 (e.g. Grinberg et al. 2014). Both the X-ray spectral properties of and all-sky monitoring data corresponding to this exposure also show that Cygnus X-1 is in the soft state (Table 2 and Figure 2). About state classification, it is worth mentioning that Cygnus X-1 has never reached the so-called thermal-dominated or soft state as defined according to BH low-mass X-ray binary phenomenology (BH LMXBs; e.g. Remillard & McClintock 2006; Belloni 2010). The X-ray spectra of the soft states of other BH LMXBs are dominated by a thermal disk component, while in Cygnus

X-1 strong Comptonization and reflection components are also significant (Walton et al. 2016; Kawano et al. 2017; Lubiński et al. 2020). Furthermore, the fractional rms amplitude measured from soft-state PDSs is usually  $\sim 20\text{--}30\%$  in Cygnus X-1 (e.g. Axelsson et al. 2006; Grinberg et al. 2014), much larger than the one measured in BH LMXBs in the thermal-dominated state. Keeping in mind these differences, we will refer to this state of Cygnus X-1 simply as the soft state.

Low-frequency QPOs are quite common in the hard state of BH XRBs. In particular, type-C QPOs are observed with fractional rms amplitude up to 20% and quality factor  $Q$  ( $\nu_0/\text{FWHM}$ )  $\geq 10$  (Casella et al. 2005; Motta 2016). Type-C QPOs are sometimes also detected in the soft state (e.g. XTE J1550–564, GRO J1655–40), but with a higher characteristic frequency ( $\geq 20$  Hz) and smaller rms amplitude than those seen in the hard state (Homan et al. 2001; Motta et al. 2012). Type-C QPOs with similar characteristics are systematically observed in most of the known BH LMXBs. However, type-C QPOs have never been detected in Cygnus X-1 observations (Belloni 2010; Ingram & Motta 2019). Pottschmidt et al. (2003) has detected weak narrow QPOs ( $\nu_0 \sim 0.1\text{--}1$  Hz) sometimes during the soft state. Rapisarda et al. (2017) also has detected a millihertz QPO ( $\nu_0 \sim 60$  mHz) during the soft state. The millihertz QPO we detected has a large quality factor  $Q$  ( $> 13$ , see  $\nu_0$  and FWHM in Table 1), which is similar to the type-C QPOs. However, its frequency and rms are smaller than most type-C QPOs observed in other BH XRBs (e.g. Motta et al. 2015). On the other hand, the rms of type-C QPOs usually increases with

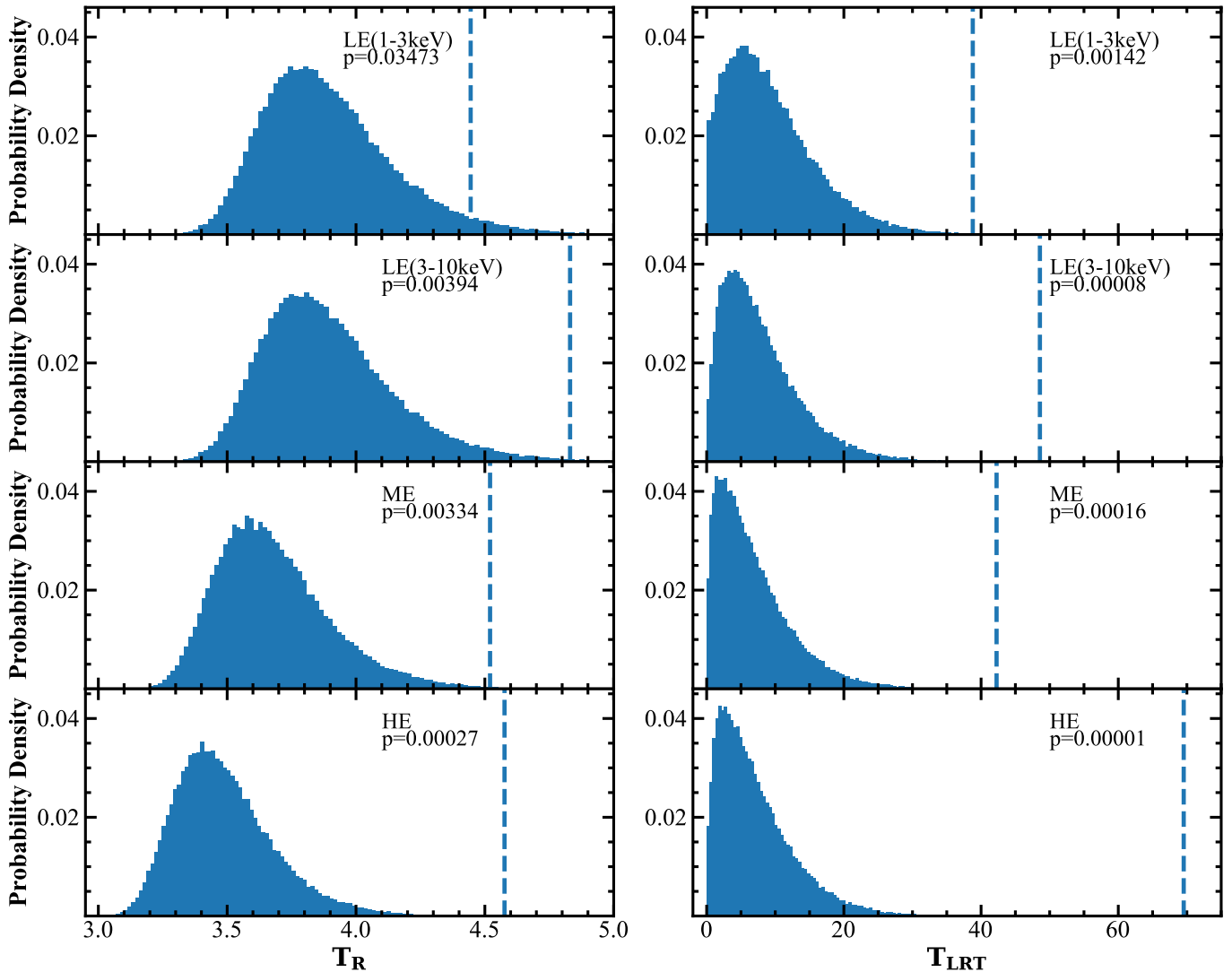


**Figure 6.** The posterior probability distributions of the test statistics  $T_R$  and  $T_{LRT}$  from the simulated sample. The dashed line marks the observed value of  $T_R$  and  $T_{LRT}$ . The posterior predictive  $p$ -value is the probability that the simulated values larger than the observed one.

photon energy and becomes constant above tens of keV (e.g. Casella et al. 2004; Huang et al. 2018), while the rms of the millihertz QPO we detected in Cygnus X-1 does not show an energy dependence above 3 keV (see Figure 4 and Table 1). Another important difference between type-C QPOs and the millihertz QPO we detected is that the former can be observed for relatively long periods of time ( $\sim$  days to tens of days), while the latter appears only in the first 12 ks of this observation. These fundamental differences suggest that the physical mechanism responsible for the observed millihertz QPO in Cygnus X-1 is different from the one producing type-C QPOs in BH LMXBs.

The origin of millihertz QPOs ( $<100$  mHz) are still not well understood, although they have been detected in different accreting systems, such as accretion-powered

X-ray pulsars (e.g. Psaltis 2006) and even ultraluminous X-ray pulsars (e.g. Feng et al. 2010), ultraluminous X-ray sources (e.g. Atapin et al. 2019) and BH XRBs (see Table 2 in Cheng et al. 2019, and references therein). In some BH LMXBs (e.g., H1743–322), millihertz QPOs and type-C QPOs are sometimes detected simultaneously and their characteristics mostly appear to be uncorrelated with each other (Altamirano & Strohmayer 2012). This supports the conclusion that in BH LMXBs the mechanism producing the millihertz QPO is not related to that producing the type-C QPO. Some of the detected millihertz QPOs appear in high-inclination systems and are thought to have similar origin as to the 1 Hz QPO in dipping neutron star XRBs (e.g. Altamirano & Strohmayer 2012; Armas Padilla et al. 2014). However, the inclination angle of the Cygnus X-1 accretion



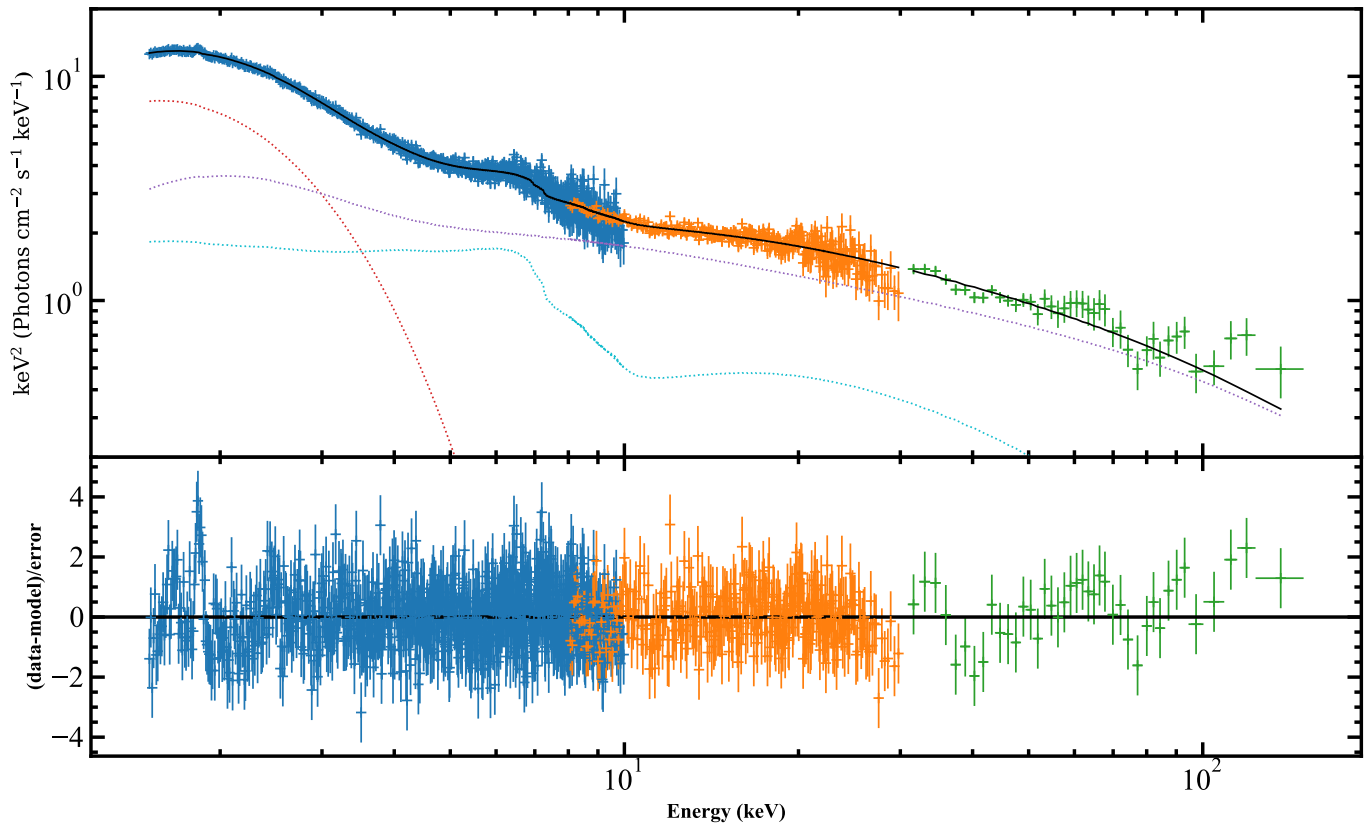


**Figure 7.** Upper panel: the unfolded spectrum of the LE (blue), ME (orange), and HE (green) and the model `const*tbabs*(diskbb+reflkerrG)` (black solid line). The dotted red, purple, and cyan lines represent the disk, Comptonization, and reflection components. Lower panel: ratio of the residual to the error of the data.

disk is estimated to be  $\sim 27^\circ$  (Orosz et al. 2011), making unlikely the relation between our detected millihertz QPO and those observed in high-inclination systems. We have noticed that the millihertz QPOs are all detected during the hard state in BH LMXBs, while they are detected during the soft state of high mass X-ray binaries (HMXB, Cheng et al. 2019), which indicates different origins in the HMXBs and LMXBs.

The millihertz QPOs in soft states have been previously observed in two other persistent BH HMXBs, namely LMC X-1 (Ebisawa et al. 1989; Alam et al. 2014) and Cyg X-3 (van der Klis & Jansen 1985; Koljonen et al. 2011; Pahari et al. 2017). The millihertz QPOs in Cyg X-3 are thought to be related to major radio flare events (Koljonen et al. 2011), which are quite unique and have not been observed in other BH XRBs, including Cygnus X-1. LMC X-1 share many common spectral and timing properties during the soft state with Cygnus X-1, even though the X-ray Eddington luminosity of Cygnus X-1 is smaller than that of LMC X-1 (e.g. Ruhlen et al. 2011) and LMC X-1 never showed transitions to the hard state. The millihertz QPO in LMC X-1 is also occasionally detected in the soft-state observations, and the frequency also varies (Ebisawa et al.

1989; Alam et al. 2014). The rare occurrence in Cygnus X-1, as well as LMC X-1, favors potential mechanisms that would only happen by chance due to some local inhomogeneity in a system embedded in a wind-accretion environment.

It has been proposed that the millihertz QPOs observed in LMC X-1 are due to global disk oscillations Titarchuk & Osherovich (2000), i.e. vertical (normal to the disk) disk oscillations triggered by the gravitational force of the central BH. The frequency of such oscillations can be estimated as

$$f_0 \approx 2 \left( \frac{R_{\text{in}}}{6R_g} \right)^{-\frac{8}{15}} \left( \frac{M_{\text{BH}}}{M_\odot} \right)^{-\frac{8}{15}} \left( \frac{P_{\text{orb}}}{3\text{hr}} \right)^{-\frac{7}{15}} \left( \frac{R_{\text{adj}}}{R_{\text{in}}} \right)^{-0.3} \text{ Hz} \quad (1)$$

where  $R_{\text{in}}$  is the inner radius of the accretion disk and  $R_{\text{adj}}$  is an adjustment radius in the disk, usually of the order of  $\sim 2-3R_{\text{in}}$  for Shakura–Sunyaev geometrically thin disks (Shakura & Sunyaev 1973; Titarchuk et al. 1998). Using  $R_{\text{adj}} = 2.5R_{\text{in}}$ ,  $P_{\text{orb}} = 5.6$  days,  $R_{\text{in}} = 2.2R_g$  (see Table 2), and  $M_{\text{BH}} = 21.2M_\odot$  (Miller-Jones et al. 2021), we obtain an oscillation frequency of  $\sim 86$  mHz, roughly consistent with the frequency of the millihertz QPO we detected. In general, the frequency of the global oscillation depends on the size of the disk

and, therefore, on both its inner and outer radius. In Equation 1, the disk is assumed to be a geometrically thin Shakura–Sunyaev disk (Shakura & Sunyaev 1973) and the outer disk radius is assumed to be half of the Roche lobe radius (Titarchuk & Osherovich 2000). In this scenario, the detection of similar millihertz QPOs at different frequencies in the same and other sources (Rapisarda et al. 2017; Alam et al. 2014) could be caused by the variation in the disk size.

However, as global disk oscillation is the vertical oscillation of the whole disk, the consequently observed modulation is expected to be from the disk emission, where it is mainly in the soft X-ray band (see Figure 7). On the other hand, global disk oscillations would be seen in other BH XRBs not limited to wind accreting systems. The fractional rms amplitude of the detected QPO persisted at a similar amplitude level at least up to 50 keV (see Figure 4), indicating that the QPO either has a hard X-ray spectrum or that the QPO originates primarily in the Comptonization component, such as certain oscillations occur in the disk corona above the standard accretion disk.

## ACKNOWLEDGMENTS

We thank Chichuan Jin and Joern Wilms for the helpful discussions. This research has made use of MAXI data provided by RIKEN, JAXA, and the MAXI team. This work was supported by part by the Natural Science Foundation of China (grants 11773055, U1838203, and U1938114), Z.Y. was also supported by the Youth Innovation Promotion Association of CAS (ids. 2020265). R.S. acknowledges the support of the PIFI fellowship of CAS under the project No. 2019PM0016 and China’s Postdoctoral International Exchange Program. W.Y. would like to acknowledge partial support by the National Program on Key Research and Development Project (grant No. 2016YFA0400804).

*Facilities:* Insight-HXMT

*Software:* astropy (Astropy Collaboration et al. 2013), stingray (Huppenkothen et al. 2019), XSPEC (Arnaud 1996)

## REFERENCES

- Alam, M. S., Dewangan, G. C., Belloni, T., Mukherjee, D., & Jhingan, S. 2014, *Monthly Notices of the Royal Astronomical Society*, 445, 4259, doi: [10.1093/mnras/stu2048](https://doi.org/10.1093/mnras/stu2048)
- Albert, J., Aliu, E., Anderhub, H., et al. 2007, *The Astrophysical Journal Letters*, 665, L51, doi: [10.1086/521145](https://doi.org/10.1086/521145)
- Altamirano, D., & Strohmayer, T. 2012, *The Astrophysical Journal*, 754, L23, doi: [10.1088/2041-8205/754/2/L23](https://doi.org/10.1088/2041-8205/754/2/L23)
- Atapin, K., Fabrika, S., & Caballero-García, M. D. 2019, *MNRAS*, 486, 2766. doi: [10.1093/mnras/stz1027](https://doi.org/10.1093/mnras/stz1027)
- Armas Padilla, M., Wijnands, R., Altamirano, D., et al. 2014, *Monthly Notices of the Royal Astronomical Society*, 439, 3908, doi: [10.1093/mnras/stu243](https://doi.org/10.1093/mnras/stu243)
- Arnaud, K. A. 1996, in *Astronomical Data Analysis Software and Systems V*, Vol. 101, 17. <http://adsabs.harvard.edu/abs/1996ASPC..101...17A>
- Astropy Collaboration, Robitaille, T. P., Tollerud, E. J., et al. 2013, *Astronomy and Astrophysics*, 558, A33, doi: [10.1051/0004-6361/201322068](https://doi.org/10.1051/0004-6361/201322068)
- Axelsson, M., Borgonovo, L., & Larsson, S. 2005, *Astronomy and Astrophysics*, 438, 999, doi: [10.1051/0004-6361:20042362](https://doi.org/10.1051/0004-6361:20042362)
- . 2006, *Astronomy and Astrophysics*, 452, 975, doi: [10.1051/0004-6361:20054397](https://doi.org/10.1051/0004-6361:20054397)
- Belloni, T., & Hasinger, G. 1990, *A&A*, 227, L33
- Belloni, T., Psaltis, D., & van der Klis, M. 2002, *The Astrophysical Journal*, 572, 392, doi: [10.1086/340290](https://doi.org/10.1086/340290)
- Belloni, T. M. 2010, in *The Jet Paradigm - From Microquasars to Quasars*, Vol. 794, eprint: arXiv:0909.2474, 53, doi: [10.1007/978-3-540-76937-8\\_3](https://doi.org/10.1007/978-3-540-76937-8_3)
- Belloni, T. M., & Stella, L. 2014, *Space Science Reviews*, 183, 43, doi: [10.1007/s11214-014-0076-0](https://doi.org/10.1007/s11214-014-0076-0)
- Bolton, C. T. 1972, *Nature*, 235, 271, doi: [10.1038/235271b0](https://doi.org/10.1038/235271b0)
- Bowyer, S., Byram, E. T., Chubb, T. A., & Friedman, H. 1965, *Science*, 147, 394, doi: [10.1126/science.147.3656.394](https://doi.org/10.1126/science.147.3656.394)
- Casella, P., Belloni, T., Homan, J., & Stella, L. 2004, *Astronomy and Astrophysics*, 426, 587, doi: [10.1051/0004-6361:20041231](https://doi.org/10.1051/0004-6361:20041231)
- Casella, P., Belloni, T., & Stella, L. 2005, *The Astrophysical Journal*, 629, 403, doi: [10.1086/431174](https://doi.org/10.1086/431174)
- Cheng, Z., Méndez, M., Altamirano, D., Beri, A., & Wang, Y. 2019, *Monthly Notices of the Royal Astronomical Society*, 482, 550, doi: [10.1093/mnras/sty2695](https://doi.org/10.1093/mnras/sty2695)
- Cui, W., Heindl, W. A., Rothschild, R. E., et al. 1997a, *The Astrophysical Journal Letters*, 474, L57, doi: [10.1086/310419](https://doi.org/10.1086/310419)
- Cui, W., Zhang, S. N., Focke, W., & Swank, J. H. 1997b, *The Astrophysical Journal*, 484, 383, doi: [10.1086/304341](https://doi.org/10.1086/304341)
- Done, C., Gierliński, M., & Kubota, A. 2007, *Astronomy and Astrophysics Review*, 15, 1, doi: [10.1007/s00159-007-0006-1](https://doi.org/10.1007/s00159-007-0006-1)

- Ebisawa, K., Mitsuda, K., & Inoue, H. 1989, *Publications of the Astronomical Society of Japan*, 41, 519.  
<http://adsabs.harvard.edu/abs/1989PASJ...41..519E>
- Fabian, A. C., Wilkins, D. R., Miller, J. M., et al. 2012, *Monthly Notices of the Royal Astronomical Society*, 424, 217, doi: [10.1111/j.1365-2966.2012.21185.x](https://doi.org/10.1111/j.1365-2966.2012.21185.x)
- Feng, H., Rao, F., & Kaaret, P. 2010, *ApJL*, 710, L137.  
doi:[10.1088/2041-8205/710/2/L137](https://doi.org/10.1088/2041-8205/710/2/L137)
- Foreman-Mackey, D., Hogg, D. W., Lang, D., & Goodman, J. 2013, *Publications of the Astronomical Society of the Pacific*, 125, 306, doi: [10.1086/670067](https://doi.org/10.1086/670067)
- Gallo, E., Fender, R., Kaiser, C., et al. 2005, *Nature*, 436, 819, doi: [10.1038/nature03879](https://doi.org/10.1038/nature03879)
- Gierliński, M., Zdziarski, A. A., Poutanen, J., et al. 1999, *Monthly Notices of the Royal Astronomical Society*, 309, 496, doi: [10.1046/j.1365-8711.1999.02875.x](https://doi.org/10.1046/j.1365-8711.1999.02875.x)
- Grinberg, V., Hell, N., Pottschmidt, K., et al. 2013, *Astronomy and Astrophysics*, 554, A88,  
doi: [10.1051/0004-6361/201321128](https://doi.org/10.1051/0004-6361/201321128)
- Grinberg, V., Pottschmidt, K., Böck, M., et al. 2014, *Astronomy and Astrophysics*, 565, A1,  
doi: [10.1051/0004-6361/201322969](https://doi.org/10.1051/0004-6361/201322969)
- Herrero, A., Kudritzki, R. P., Gabler, R., Vilchez, J. M., & Gabler, A. 1995, *Astronomy and Astrophysics*, 297, 556.  
<http://adsabs.harvard.edu/abs/1995A%26A...297..556H>
- Homan, J., Wijnands, R., van der Klis, M., et al. 2001, *The Astrophysical Journal Supplement Series*, 132, 377,  
doi: [10.1086/318954](https://doi.org/10.1086/318954)
- Huang, Y., Qu, J. L., Zhang, S. N., et al. 2018, *The Astrophysical Journal*, 866, 122,  
doi: [10.3847/1538-4357/aade4c](https://doi.org/10.3847/1538-4357/aade4c)
- Huppenkothen, D., Younes, G., Ingram, A., et al. 2017, *The Astrophysical Journal*, 834, 90,  
doi: [10.3847/1538-4357/834/1/90](https://doi.org/10.3847/1538-4357/834/1/90)
- Huppenkothen, D., Bachetti, M., Stevens, A. L., et al. 2019, *The Astrophysical Journal*, 881, 39,  
doi: [10.3847/1538-4357/ab258d](https://doi.org/10.3847/1538-4357/ab258d)
- Ingram, A. R., & Motta, S. E. 2019, *New Astronomy Reviews*, 85, 101524, doi: [10.1016/j.newar.2020.101524](https://doi.org/10.1016/j.newar.2020.101524)
- Israel, G. L., & Stella, L. 1996, *The Astrophysical Journal*, 468, 369, doi: [10.1086/177697](https://doi.org/10.1086/177697)
- Kantzas, D., Markoff, S., Beuchert, T., et al. 2021, *Monthly Notices of the Royal Astronomical Society*, 500, 2112,  
doi: [10.1093/mnras/staa3349](https://doi.org/10.1093/mnras/staa3349)
- Kawano, T., Done, C., Yamada, S., et al. 2017, *Publications of the Astronomical Society of Japan*, 69, 36, doi: [10.1093/pasj/psx009](https://doi.org/10.1093/pasj/psx009)
- Koljonen, K. I. I., Hannikainen, D. C., & McCollough, M. L. 2011, *Monthly Notices of the Royal Astronomical Society*, 416, L84, doi: [10.1111/j.1745-3933.2011.01104.x](https://doi.org/10.1111/j.1745-3933.2011.01104.x)
- Krimm, H. A., Holland, S. T., Corbet, R. H. D., et al. 2013, *The Astrophysical Journal Supplement Series*, 209, 14,  
doi: [10.1088/0067-0049/209/1/14](https://doi.org/10.1088/0067-0049/209/1/14)
- Leahy, D. A., Elsner, R. F., & Weisskopf, M. C. 1983, *The Astrophysical Journal*, 272, 256, doi: [10.1086/161288](https://doi.org/10.1086/161288)
- Li, X., Li, X., Tan, Y., et al. 2020, *Journal of High Energy Astrophysics*, 27, 64, doi: [10.1016/j.jheap.2020.02.009](https://doi.org/10.1016/j.jheap.2020.02.009)
- Lubiński, P., Filothodoros, A., Zdziarski, A. A., & Pooley, G. 2020, *The Astrophysical Journal*, 896, 101,  
doi: [10.3847/1538-4357/ab9311](https://doi.org/10.3847/1538-4357/ab9311)
- Matsuoka, M., Kawasaki, K., Ueno, S., et al. 2009, *Publications of the Astronomical Society of Japan*, 61, 999, doi: [10.1093/pasj/61.5.999](https://doi.org/10.1093/pasj/61.5.999)
- Miller-Jones, J. C. A., Bahramian, A., Orosz, J. A., et al. 2021, *arXiv e-prints*, 2102, arXiv:2102.09091.  
<http://adsabs.harvard.edu/abs/2021arXiv210209091M>
- Motta, S., Homan, J., Muñoz Darias, T., et al. 2012, *Monthly Notices of the Royal Astronomical Society*, 427, 595, doi: [10.1111/j.1365-2966.2012.22037.x](https://doi.org/10.1111/j.1365-2966.2012.22037.x)
- Motta, S. E. 2016, *Astronomische Nachrichten*, 337, 398,  
doi: [10.1002/asna.201612320](https://doi.org/10.1002/asna.201612320)
- Motta, S. E., Casella, P., Henze, M., et al. 2015, *Monthly Notices of the Royal Astronomical Society*, 447, 2059,  
doi: [10.1093/mnras/stu2579](https://doi.org/10.1093/mnras/stu2579)
- Niedźwiecki, A., Szanecki, M., & Zdziarski, A. A. 2019, *Monthly Notices of the Royal Astronomical Society*, 485, 2942, doi: [10.1093/mnras/stz487](https://doi.org/10.1093/mnras/stz487)
- Nowak, M. A., Vaughan, B. A., Wilms, J., Dove, J. B., & Begelman, M. C. 1999, *The Astrophysical Journal*, 510, 874, doi: [10.1086/306610](https://doi.org/10.1086/306610)
- Orosz, J. A., McClintock, J. E., Aufdenberg, J. P., et al. 2011, *The Astrophysical Journal*, 742, 84,  
doi: [10.1088/0004-637X/742/2/84](https://doi.org/10.1088/0004-637X/742/2/84)
- Pahari, M., McHardy, I. M., Mallick, L., Dewangan, G. C., & Misra, R. 2017, *Monthly Notices of the Royal Astronomical Society*, 470, 3239,  
doi: [10.1093/mnras/stx1455](https://doi.org/10.1093/mnras/stx1455)
- Psaltis, D. 2006, *Compact stellar X-ray sources*, 1
- Paul, B., Agrawal, P. C., & Rao, A. R. 1998, *Journal of Astrophysics and Astronomy*, 19, 55,  
doi: [10.1007/BF02714891](https://doi.org/10.1007/BF02714891)
- Pottschmidt, K., Wilms, J., Nowak, M. A., et al. 2003, *Astronomy and Astrophysics*, 407, 1039,  
doi: [10.1051/0004-6361:20030906](https://doi.org/10.1051/0004-6361:20030906)
- Poutanen, J., & Svensson, R. 1996, *The Astrophysical Journal*, 470, 249, doi: [10.1086/177865](https://doi.org/10.1086/177865)
- Rapisarda, S., Ingram, A., & van der Klis, M. 2017, *Monthly Notices of the Royal Astronomical Society*, 472, 3821, doi: [10.1093/mnras/stx2110](https://doi.org/10.1093/mnras/stx2110)

- Remillard, R. A., & McClintock, J. E. 2006, *Annual Review of Astronomy and Astrophysics*, 44, 49, doi: [10.1146/annurev.astro.44.051905.092532](https://doi.org/10.1146/annurev.astro.44.051905.092532)
- Ruhlen, L., Smith, D. M., & Swank, J. H. 2011, *The Astrophysical Journal*, 742, 75, doi: [10.1088/0004-637X/742/2/75](https://doi.org/10.1088/0004-637X/742/2/75)
- Shakura, N. I., & Sunyaev, R. A. 1973, *Astronomy and Astrophysics*, 24, 337. <http://adsabs.harvard.edu/abs/1973A%26A...24..337S>
- Shaposhnikov, N., & Titarchuk, L. 2006, *The Astrophysical Journal*, 643, 1098, doi: [10.1086/503272](https://doi.org/10.1086/503272)
- Tananbaum, H., Gursky, H., Kellogg, E., Giacconi, R., & Jones, C. 1972, *The Astrophysical Journal Letters*, 177, L5, doi: [10.1086/181042](https://doi.org/10.1086/181042)
- Titarchuk, L., Lapidus, I., & Muslimov, A. 1998, *The Astrophysical Journal*, 499, 315, doi: [10.1086/305642](https://doi.org/10.1086/305642)
- Titarchuk, L., & Osherovich, V. 2000, *The Astrophysical Journal Letters*, 542, L111, doi: [10.1086/312935](https://doi.org/10.1086/312935)
- Tomsick, J. A., Nowak, M. A., Parker, M., et al. 2014, *The Astrophysical Journal*, 780, 78, doi: [10.1088/0004-637X/780/1/78](https://doi.org/10.1088/0004-637X/780/1/78)
- van der Klis, M. 1989, in *Timing Neutron Stars: proceedings of the NATO Advanced Study Institute on Timing Neutron Stars*, Vol. 262, 27. <http://adsabs.harvard.edu/abs/1989ASIC..262...27V>
- van der Klis, M., & Jansen, F. A. 1985, *Nature*, 313, 768, doi: [10.1038/313768a0](https://doi.org/10.1038/313768a0)
- Vaughan, S. 2005, *Astronomy and Astrophysics*, 431, 391, doi: [10.1051/0004-6361:20041453](https://doi.org/10.1051/0004-6361:20041453)
- . 2010, *Monthly Notices of the Royal Astronomical Society*, 402, 307, doi: [10.1111/j.1365-2966.2009.15868.x](https://doi.org/10.1111/j.1365-2966.2009.15868.x)
- Verner, D. A., Ferland, G. J., Korista, K. T., & Yakovlev, D. G. 1996, *The Astrophysical Journal*, 465, 487, doi: [10.1086/177435](https://doi.org/10.1086/177435)
- Walton, D. J., Tomsick, J. A., Madsen, K. K., et al. 2016, *The Astrophysical Journal*, 826, 87, doi: [10.3847/0004-637X/826/1/87](https://doi.org/10.3847/0004-637X/826/1/87)
- Webster, B. L., & Murdin, P. 1972, *Nature*, 235, 37, doi: [10.1038/235037a0](https://doi.org/10.1038/235037a0)
- Wijnands, R., Homan, J., & van der Klis, M. 1999, *The Astrophysical Journal Letters*, 526, L33, doi: [10.1086/312365](https://doi.org/10.1086/312365)
- Wilms, J., Allen, A., & McCray, R. 2000, *The Astrophysical Journal*, 542, 914, doi: [10.1086/317016](https://doi.org/10.1086/317016)
- Yuan, F., & Narayan, R. 2014, *Annual Review of Astronomy and Astrophysics*, 52, 529, doi: [10.1146/annurev-astro-082812-141003](https://doi.org/10.1146/annurev-astro-082812-141003)
- Zdziarski, A. A., Johnson, W. N., & Magdziarz, P. 1996, *Monthly Notices of the Royal Astronomical Society*, 283, 193, doi: [10.1093/mnras/283.1.193](https://doi.org/10.1093/mnras/283.1.193)
- Zhang, S.-N., Li, T., Lu, F., et al. 2020, *Science China Physics, Mechanics, and Astronomy*, 63, 249502, doi: [10.1007/s11433-019-1432-6](https://doi.org/10.1007/s11433-019-1432-6)
- Zhao, X., Gou, L., Dong, Y., et al. 2021, arXiv e-prints, 2102, arXiv:2102.09093. <http://adsabs.harvard.edu/abs/2021arXiv210209093Z>
- Zhao, X.-S., Dong, Y.-T., Gou, L.-J., et al. 2020, *Journal of High Energy Astrophysics*, 27, 53, doi: [10.1016/j.jheap.2020.03.001](https://doi.org/10.1016/j.jheap.2020.03.001)